HEFAT2012
9th International Conference on Heat Transfer, Fluid Mechanics and Thermodynamics
16 – 18 July 2012
Malta

THREE-DIMENSIONAL FLOW STRUCTURE BEHIND AN AHMED VEHICLE MODEL

Wang X W[1,2], Zhou Y[1,]*, Pin Y F[1], Chan T L[1]
[1]Department of Mechanical Engineering, The Hong Kong Polytechnic University, Hong Kong
[#]Engineering Research Center for Sensors and Measurements, 66 Huangshan Rd, Chongqing
*Corresponding author: mmyzhou@inet.polyu.edu.hk

ABSTRACT

The lasting high fuel cost has recently inspired resurgence in drag reduction research for vehicles, which calls for a thorough understanding of the vehicle wake. The simplified Ahmed vehicle model is characterized by controllable flow separation, thus especially suitable for this purpose. In spite of a considerable number of previous investigations, our knowledge of flow around this model remains incomplete. This work aims to revisit turbulent flow structure behind this model. Two rear slant angles, i.e., α = 25º and 35º, of the model were examined, representing two distinct flow regimes. The Reynolds number was 5.26×10^4 based on the model height (H) and incident flow velocity. Using particle image velocimetry (PIV), flow was measured with and without a gap (g/H = 0.174) between the vehicle underside and ground in three orthogonal planes, viz. the x-z, x-y and y-z planes, where x, y and z are the coordinates along longitudinal, transverse and spanwise directions, respectively. The flow at g/H = 0 serves as an important reference for the understanding of the highly complicated vehicle wake ($g/H \neq 0$). While reconfirming the well documented major characteristics of the mean flow structure, both instantaneous and time-averaged PIV data unveil a number of important features of the flow structure, which have not been previously reported. As such, considerably modified flow structure models are proposed for both regimes. The time-averaged velocities, second moments of fluctuating velocities and vorticity components are presented and discussed, along with their dependence on g/H in the two distinct flow regimes.

1. INTRODUCTION

The global warming and lasting high fuel costs in the past few years highlight the necessity and urgency of drag reduction research for vehicles, which warrants a thorough understanding of the flow around vehicles because of a connection between the flow structure and aerodynamic drag. Past studies have unveiled that the pressure drag contributes predominantly to the total drag acting on vehicles, in particular at a high speed. The pressure drag is generated largely by the after-body for most cars, with little contribution from the fore-body [1] and is directly linked to the coherent structures in the vehicle wake [2]. As such, the wake of three-dimensional (3-D) vehicle models has caught considerable attention in the past because of its fundamental and engineering significance [3]; a large number of experimental and numerical investigations have been performed since the pioneer work of Janssen and Hucho[4].

The so-called Ahmed body[5] is perhaps the most widely studied simplified car model, which is a 3-D bluff body. Its blunt forebody is designed to avoid separation so that the aerodynamic forces depend largely on the flow structure created on its after-body. This flow structure is unsteady, very complicated, and highly 3-D, including three major components: a recirculation bubble over the rear slanted surface, longitudinal vortices originating from the two side edges or C-pillars of the surface and a recirculation torus in the base of the model. The strength and behaviors of the three types of coherent structures and their interactions depend on the slant angle (α) of the upper rear surface of the model [5]. Please refer Figure 1 for the definitions of α and the present coordinate system. At smallα, the flow is characterized by two counter-rotating longitudinal vortices [6]. The vortices produce drag on one hand and induce a downwash between them, which enhances flow attachment on the slanted surface, on the other hand. The net effect is a drag reduction. The minimum drag occurs at α = 12.5°. The flow at this α appears to be "two-dimensional" (2-D) except in the vicinity of the two C-pillars of the surface. This is evident from the parallel isobars of static pressure running across the surface [5]. Beyond $\alpha \approx 15°$, the flow over the rear slanted surface becomes highly 3-D. The pressure drag rises rapidly with increasing α and reaches the maximum at α = 30°, where the two longitudinal vortices achieve their maximum strength. At $\alpha > 30°$, the flow is dominated by spanwise vortices with the longitudinal vortices burst, and the pressure drag falls despite a fully separated flow. Apparently, α = 30° is a division point for two distinct regimes[1]. The flow is highly sensitive to a small change in α at the critical configuration. This is evident in Sims-Williams's detailed study of the time-averaged and unsteady flow structures at α = 30° based on 5-hole probe and smoke flow visualization measurements [7, 8].

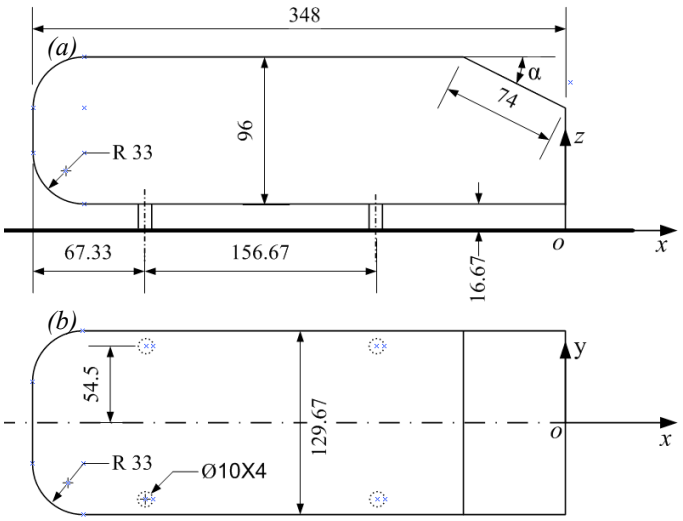

Figure 1 Dimensions of the scaled-down Ahmed vehicle model and the definition of the coordinate system: (a) side view, (b) plan view. The length unit is mm and angle is in degree.

Previous studies have greatly advanced our understanding of the flow structure behind the Ahmed model and meanwhile raised a number of issues to be resolved or clarified. For example, flow structure models were proposed, which are different from the well known model shown in Ahmed *et al*.[5] Vino *et al*.[9] investigated experimentally flow structures in the near-wake of the Ahmed model (α = 30°) using a 13-hole probe, which allowed reliable measurements in regions exhibiting large flow angles, including flow reversals. Their time-averaged results showed good agreement with previously published data at x/H = 1.09 but not at 0.044, much of inconsistency being connected to interactions between the separated flow over the slant and the recirculatory flow in the vertical base of the vehicle model. Their detached flow over the slant was not fully reattached, in deviation from what Ahmed *et al*. [5] suggested; that is, the flow above the central region of the slant was reattached, forming a separation bubble, before separating again from the base.

The well-known wake structure model for α < 30° is characterized by one pair of counter-rotating longitudinal vortices. However, Krajnovic *et al.*'s numerical simulation[10] of the Ahmed vehicle model at α = 25° with *g/H* = 0.174 pointed to the presence of one more pair of counter-rotating longitudinal vortices near the lower corner of the side surface, though Krajnovic *et al.*[10] considered the vortices to be too weak to be of aerodynamic significance. In this paper, *g* denotes the gap separation between the ground surface and the model underside and *H* represents the model height. Strachan *et al*. [11] measured using LDA time-averaged velocities behind an Ahmed vehicle model of α = 0° ~ 40°, which was supported on an overhead aerodynamic strut. They observed at *g/H* = 0.174 a shear layer near the lower side edge of the model, thus also inferring the presence of one pair of counter-rotating longitudinal vortices, which were referred to as "lower vortices" to be distinguished from the C-pillar vortices. This pair of lower vortices was not reported previously, for example, by Ahmed *et al*.[5], Sims-Williams & Duncan[12] and Vino *et al.*[9], who used a 10-hole, a 5-hole and a 13-hole directional probe, respectively, nor by Lienhart *et al*.[13], who also used an LDA technique. Strachan *et al*.[11] ascribed this discrepancy to the use of cylindrical struts used in the earlier investigations and suggested that the struts suppress the formation of the lower vortices. This has been demonstrated to be incorrect in the present investigation. The mechanism behind the lower vortex generation and the dynamic role of this vortex needs to be clarified.

One may wonder whether the discrepancy mentioned above has anything to do with g/H ($\neq$ 0) due to the presence of wheels. Krajnovic & Davidson[14] observed flow separation at the leading lower edge of the vehicle model with *g/H* = 0.174, but not in their earlier studies of a similar vehicle model with *g/H* = 0.08[15,16]. They subsequently linked the different observations to the clearance effect. So far, this effect on the vehicle aerodynamics has not been given adequate attention in the literature. Furthermore, the extreme case at *g/H* = 0 excludes the effect of the gap and hence the coherent structures, e.g. bubble "B", associated with the gap, do not occur, thus eliminating the complication due to the presence of this gap and providing a valuable reference for the understanding of the flow physics.

With the above issues identified in mind, the first objective of this work is to gain through measurements a better picture of the flow structure around the Ahmed vehicle model; the second is to investigate the effect of the clearance between the model underside and the ground surface on the flow structure; the third is to provide the experimental data of the second order moments of fluctuating velocities as well as the mean velocity field for numerical modeling. Two configurations, i.e., α = 25º and 35º, were investigated, corresponding to the two distinct flow regimes [5, 1]. In view of a highly 3-D flow, the PIV measurements were conducted in three orthogonal planes behind the model with and without a clearance between the model underside and the wind tunnel wall. Based on the data obtained, the instantaneous and time-averaged flow fields are examined and discussed, along with the Reynolds stresses and also published results, including the variants of proposed flow structure models.

2. EXPERIMENTAL DETAILS

2.1 Wind tunnel and vehicle model

Experiments were carried out in a closed circuit wind tunnel with a 2.4-m-long square test section (0.6 m x 0.6 m). The flow non-uniformity in the test section is 0.1% and the streamwise turbulence intensity is less than 0.4% in the absence of the vehicle model for the velocity range examined presently. The working section wall was made of optical glass in order to enhance the signal-to-noise ratio in PIV measurements. See Huang *et al*.[17] for more details of the tunnel. The dimensions of a 1/3-scaled Ahmed vehicle model are given in Figure 2. Two angles, i.e. α = 25° and 35°, were investigated. The model is 0.348 m in length (*L*), 0.13 m in width (*B*), and 0.096m in *H,* placed on a flat plate (length x width x thickness = 2 m x 0.59

m x 0.02 m) raised from the floor of the working section. The four wheels of the model were simulated by four 16.67-mm-tall struts with a diameter of 10 mm. The front end of the model was 0.3 m downstream of the leading edge of the plate. The blockage ratio of the frontal surface of the model to the rectangular test section above the flat plate was around 4.1%, not exceeding 5%, a suggested limit beyond which the blockage effect cannot be neglected [18]. The leading edge of the plate was a clipper-built curve, following Narasimha and Prasad's design [19], to avoid flow separation. Measurements were conducted at the free-stream velocity U_∞= 8.33 m/s, corresponding to a Reynolds number, $Re_H \equiv U_\infty H/\nu = 0.53\times10^5$, where ν is the kinematic viscosity of air. The Re_H effect on the flow will not be investigated in this paper, though not systematically documented in the literature. However, the design of the Ahmed model has ensured minimized flow separation from its fore-body and fixed flow separation from its after-body owing to the clearly defined corners, especially at relatively large α of present concern; as such, the wake of the model is not expected to be strongly dependent on Re_H. Indeed, limited data indicates that the drag coefficient and Strouhal number vary only slightly with increasing Re_H.[9,20,21]

The coordinate system (Fig 1) follows the right-hand rule and is defined such that *x, y* and *z* are directed along the mean flow, vertical (transverse), and spanwise directions, respectively. In this paper, asterisk denotes normalization by *H* and/or U_∞, e.g. $x^*= x/H$, $y^* = y/H$ and $z^* = z/H$. The instantaneous velocity components in the *x*, *y* and *z* directions are designated as *U*, *V* and *W*, respectively.

2.2 Documentation of boundary layer

The boundary layer over the plate may have an effect on the flow structure around a finite-height bluff body[22]. It is therefore important to document the conditions of the boundary layer, where the model was placed. An LDA system (Dantec Model 58N40) with an enhanced flow velocity analyzer was used to measure $\overline{U}$ and u_{rms} at 0.3 m from the leading edge of the plate in the plane of symmetry. The flow was seeded by smoke generated from paraffin oil with an averaged particle size of around 1μm in diameter. The measuring volume of the LDA system had a major axis of 2.48 mm and a minor axis of 1.18 mm. More than 5,000 instantaneous samples were collected at each point.

2.3 PIV measurements

A DANTEC standard PIV system was used to measure flow around the Ahmed model with and without the four struts (wheels), i.e. $g^* = 0.174$ and 0, in order to understand the effect of the clearance between the model underside and wall on the flow structure. The schematic of experimental setup is shown in Figure 2. The same seeding was used as in the LDA measurement. Flow illumination was provided by two Newwave standard pulsed laser sources of 532nm wavelength, each with a maximum energy output of 120mJ/pulse. Each laser pulse lasted for 0.01 μs. Particle images were taken using a CCD camera (HiSense type 4M, double frames, 2048×2048 pixels). Synchronization between image taking and flow illumination was provided by the Dantec FlowMap processor (System HUB).

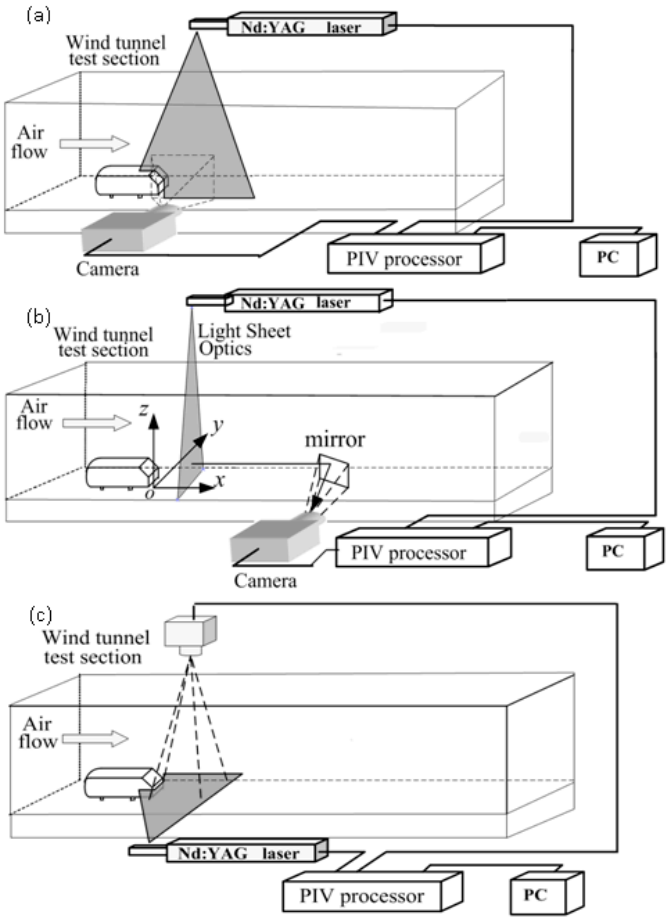

Figure 2 PIV measurement arrangements in (a) the *x-z* plane, (b) *y-z* plane, and (c) *x-y* plane.

The flow is highly three-dimensional [5]. In order to capture accurately the flow structure, one should ideally conduct measurements around the model in a large number of planes along each of the x, y and z directions. This is unpractical because of the demands for a tremendous storage space of data and also an exhaustive amount of time and effort for data analysis. Therefore, PIV measurements were performed in a limited number of planes, including the *x-z* plane at $y^* = 0$ (symmetry plane), the *x-y* plane at mid-height of the model from wall, i.e. $z^* = 0.59$ at $g^* = 0.174$ or $z^* = 0.5$ at $g^* = 0$, and the *y-z* plane at $x^*= 0.23$ and 5.00, one in the near wake and the other in the far wake, i.e., within and outside the recirculation region, respectively. Different measurement planes are illustrated in Figure 2. For the measurements in the *y-z* plane, a mirror of 120 mm ×120 mm was vertically placed at $x/H = 15$ in the tunnel, whose normal direction was 135° from the x axis. At such a distance downstream of the PIV imaging plane, the camera should have a negligibly small effect on measurement [23]. The PIV images covered an area of 2.4H × 2.4H ($x^* = -0.6 \sim 1.8$, $z^* = -0.15 \sim 2.25$), 2.4H × 2.4H ($y^* = -1.2 \sim 1.2$, $z^* = -0.2 \sim 2.2$), and 1.96H × 1.96H ($x^* = -0.06 \sim 1.9$, $y^* = -0.98 \sim$

0.98) for the *x-z*, *y-z* and *x-y* planes, respectively. The image magnifications in both directions of the plane were identical, ranging from 103 to 113 μm/pixel. The interval between two successive pulses was set at 50 μs for measurements in the *x-y* and *x-z* planes, during which fluid particles may travel a distance of 0.42 mm at $U_\infty = 8.33 m/s$. Following Huang *et al*.[17], the laser sheet was made thicker for measurements in the *y-z* plane, i.e., 3 mm (cf. 1.0~1.5 mm in the *x-y* and *x-z* planes) in order to capture the maximum number of seeding particles during each pulse.

In processing PIV images, 32 × 32 interrogation areas were used with a 50% overlap in each direction, producing 127 × 127 in-plane velocity vectors and the same number of vorticity components $\Omega_x = \overline{\Omega_x} + \omega_x$, $\Omega_y = \overline{\Omega_y} + \omega_y$ or $\Omega_z = \overline{\Omega_z} + \omega_z$ in the x, y and z directions, respectively, where ω_x , ω_y and ω_z are the fluctuating vorticity components, respectively. The vorticity data was calculated by a built-in function of the FlowMap Processor based on eight surrounding velocity data. The spatial resolution of vorticity data was about 1.81 mm, 1.81 mm and 1.66 mm for the *x-z, y-z,* and *x-y* planes, respectively. A total of 1100 PIV images were captured in each plane. The number of images has to be adequate for both mean and fluctuating flow fields.

3. LONGITUDINAL STRUCTURE

3.1 Time-averaged flow

The wake of the Ahmed vehicle model is characterized by predominantly longitudinal structures that play a crucial role in determining aerodynamic forces[5]. Naturally, the longitudinal structures have been a focus in previous experimental investigations, most of which were performed based on time-averaged data perhaps due to a limitation in measurement techniques. As such,time-averaged data is presently examined first to facilitate data comparison and interpretation. Figure 3 compares the iso-contours of $\overline{\Omega_x^*}$ in the *y-z* plane at $x^* = 0.23$ with and without a gap of $g^* = 0.174$ for $\alpha = 25°$ and 35°. The same cutoff contour level and increment are used in the four plots of Fig 3 and those following to facilitate comparison. The flow structure appears highly complicated, displaying many vorticity concentrations, as noted by Bearman[13]. A close inspection of the contours unveils interesting details on the flow structure, as well as the major flow characteristics that conform to previous numerical and experimental studies[5,7,9,13,10,24] .

At $\alpha = 25°$ (figure 3a), a number of observations can be made. Firstly, the two most concentrated longitudinal vortices, marked by "C", are well known C-pillar vortices. Their centres are located at (y^*, z^*) ≈ (- 0.56, 0.9) and (0.52, 0.9), respectively. With flow blowing over the vehicle body, the shear layers over the C-pillars roll up into the longitudinal or C-pillar vortices. Secondly, there are many vorticity concentrations behind the model vertical base, which tend to be aligned in two rows, one at the same level of the upper edge of the base and the other right above the lower edge. These structures probably result from the shear layer separation from the upper and lower edges, that is, they are associated with the two recirculatory bubbles, one above the other, and referred to as vortices "A" and "B" by Ahmed *et al*.[5]. The signs of the structures near the upper edge tend to occur alternately, which have not been reported previously and will be discussed later in detail together with instantaneous vorticity contours. Thirdly, the central region "E" of the slant surface is not associated with large vorticity concentrations. This should be reasonable. Compared with the case of $\alpha < 12.5°$ where flow over the slant surface is rather 2-D and fully attached to the surface[5], the two longitudinal vortices for $12.5° < \alpha \leq 30°$ grow in size, resulting in a 3-D flow over the slant surface and meanwhile maintaining attached flow over a section of the surface[11], though the flow separates from and reattaches on the slant surface, forming a separation bubble, when α is close to 30°. Fourthly, a number of concentrations show up above the C-pillar vortices. As will be seen later from the data in the *x-z* plane, the shear layer developed over the top surface of the model does not entirely remain attached to the slant; rather, part of it shoots over, deviating only slightly from the horizontal direction. The detached shear layer, under the rolling effect of C-pillar vortices, is probably responsible for the concentrations. Fifthly, Figure 3a displays one additional pair of counter-rotating longitudinal vortices, marked by "H", which occur near the lower corners of the model, one at (y^*, z^*) ≈ (- 0.88, 0.16) and the other at (y^*, z^*) ≈ (0.80, 0.16). Their maximum vorticity concentration is about 5% of the C-pillar vortex. Most previous measurements using multi-hole probes, hotwires or LDA failed to capture the two vortices. The first observation was made by Krajnovic *et al.*[10] based on their LES data at $\alpha = 25°$, who considered the vortices to be too weak to be of any aerodynamic significance. Stranchen *et al*.[11] made a similar observation based on their LDA data. With their model supported by a single overhead strut, they ascribed the generation of the vortices to four cylindrical struts used in many earlier measurements. A different opinion is offered here. The presence of the boundary layers formed on the wall and the model underside decelerates fluid and hence increases the pressure of the gap flow. The iso-contours of $\overline{V^*}$ in the *y-z* plane (not shown) indicate a flow squeezed out of the gap, that is, the pressure difference between flow inside the gap and that outside induces the rollup of fluid, forming longitudinal vortices in a manner similar to the C-pillar vortices. The vortices are presently referred to as the lower vortices, following Stranchen *et al*.[11] The lower vortices are predominantly longitudinal. As a matter of fact, supplementary PIV measurements (not shown), conducted in the *x-z* plane at $y^* = -0.57$ and -0.77, failed to capture any appreciable vorticity concentration at the position where the lower vortices occur. Finally, there is one stretched vorticity concentration, marked by "I", along each side surface of the model, which originates probably from the shear layer developed over the side surface of the model.

In the absence of the gap, i.e., $g^* = 0$ (Fig 3b), there is a marked change in the flow structure. The most noticeable is perhaps the absence of the lower vortices "H", corroborating our proposition on their generation mechanism. The maximum vorticity concentrations of the C-pillar vortices "C" are increased by about 50%, though the vortex size shrinks. The vorticity concentrations generated by flow separation from the upper edge of the base, associated with recirculatory bubble "A", are evident and again occur alternately in sign. On the other hand, the lower row of concentrations could not be seen. This is reasonable since the recirculatory bubble "B" results largely from the shear layer separating from the lower edge of the vertical base and upwash flow [5,12,9]. Finally, the stretched concentrations "I" are enhanced in both size and the maximum vorticity. The changes suggest that the gap has a profound influence on the wake and hence aerodynamics of ground vehicles.

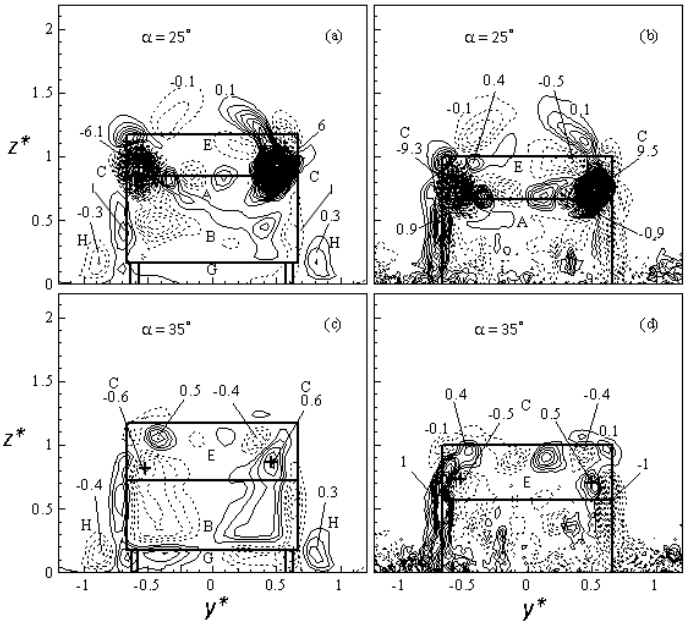

Figure 3 Iso-contours of averaged streamwise component, $\overline{\Omega_x}^*$, of vorticity in the *y*-*z* plane at $x^* = 0.23$ ($Re_H = 5.26\times 10^4$): (a, c) $g^* = 0.174$, (b, d) $g^* = 0$. The contour interval is 0.1 and the cutoff level is ± 0.1.

At $\alpha = 35°$, flow separates from the upper edge of the rear slant surface, and the C-pillar vortices burst[5]. This is reflected in Fig 3c. Firstly, there is one row of vorticity concentrations, again alternately arranged in sign, right below the upper edge of the slant. They result from flow separation and are brought down by downwash flow. Secondly, the maximum vorticity concentration of vortices "C" diminishes to about 10% of its counterpart at $\alpha = 25°$ (Fig 3a). The vortices further exhibit a significant reduction in size, though appearing enlarged due to their merging with vorticity concentrations in the base. The observation is consistent with Ahmed *et al.*'s report [5] that the separation region or half elliptic recirculation flow on the slant surface joined the separation bubble of the base so that bubbles "A" and "E" could no longer be considered to be separate. Note that the maximum concentration of the lower vortex "H" retains its strength at $\alpha = 25°$ and now amounts to about 50% of the C-pillar vortex. Naturally, its dynamic role may not be necessarily negligible. There is one pair of vortices "G" between the wall and the model underside, apparently linked to the shear layer developed in the gap and hence called the gap vortices. The gap vortex could not be seen in Fig 3a. As will be shown later, the downwash flow is markedly stronger at $\alpha = 25°$ than at $\alpha = 35°$, thus keeping the gap vortices down, without being captured at the present imaging plane.

In the absence of the gap (Fig 3d, $\alpha = 35°$), the row of alternately signed vorticity concentrations, resulting from shear layer separation from the upper edge of the slant surface, appears enhanced in strength, albeit slightly. The concentrations "I" are also strengthened. On the other hand, the C-pillar vortex is further impaired in both the maximum vorticity and size, compared to Fig 3c. So are the concentrations associated with the separation bubble in the model vertical base.

3.2 Instantaneous flow

Most of previous investigations are focused on time-averaged flow field around Ahmed vehicle model for various reasons. Many important details of the flow field could be lost or buried in the time-averaging process. There have been efforts in performing oil or smoke flow visualization to complement the data of time-averaged flow field [5,9,13]. These efforts provide flow pictures on the model surface or in the *x*-*z* plane and indeed further our understanding of flow physics. The present PIV measurements in three orthogonal planes provide us with a great opportunity to explore instantaneous flow structures off the vehicle model, in particular, in the *y*-*z* plane.

Figure 4 illustrates typical Ω_x^*-contours in the *y*-*z* plane at $x^* = 0.23$. Apparently, the instantaneous flow structure is highly complicated; the base region is packed with the vortical motions or vorticity concentrations of various scales. Nevertheless, a close inspection allows us to connect these motions to the time-averaged major features shown in Fig 3. The C-pillar vortices are easily identified in Fig 4a and 4b with the pair of the most highly concentrated counter-rotating large-scale vorticity concentrations. The lower vortices are also discernible in Fig 4a and 4c. Note that in the absence of the clearance the vorticity concentrations (Fig 4b, 4d) may occur near the lower corners of the model. However, their signs appear rather random, that is, these concentrations tend to cancel out each other in the averaging process, explaining the absence of the lower vortex in Fig 3b and 3d.

It is of interest to note that one row of four alternately signed vorticity concentrations occur between the C-pillar vortices in Fig 4a and 4b, corresponding reasonably well to the concentrations between the C-pillar vortices in Fig 3a and 3b. Absence of a negative concentration between the positive C-pillar vortex and the positive concentration at $(y^*, z^*) \approx (0.1, 0.85)$ in Fig 3a is probably due to cancellation by the random change in the size of the positive C-pillar vortex. The row of alternately signed vorticity concentrations near the lower edge

of the base in Fig 4a is also interesting, which may be associated with the recirculatory bubble "B" in the time-averaged flow field. These structures appear smaller-scaled than those right below the upper edge of the base. At $\alpha = 35°$, flow separates from the upper edge of the slant, not the upper edge of the base[5]. Therefore, the alternately signed structures could not be seen near the upper edge of the base but are evident right below the upper edge of the slant (Fig 4c, 4d), though again with relatively small scales. The observations suggest a connection between the alternately signed vortical structures and flow separation from the model. One is naturally tempted to beg the question: why do the structures associated with the recirculatory bubbles "A" and "B" tend to occur alternately in sign, which has been confirmed by many plots of instantaneous Ω_x^*-contours we have inspected?

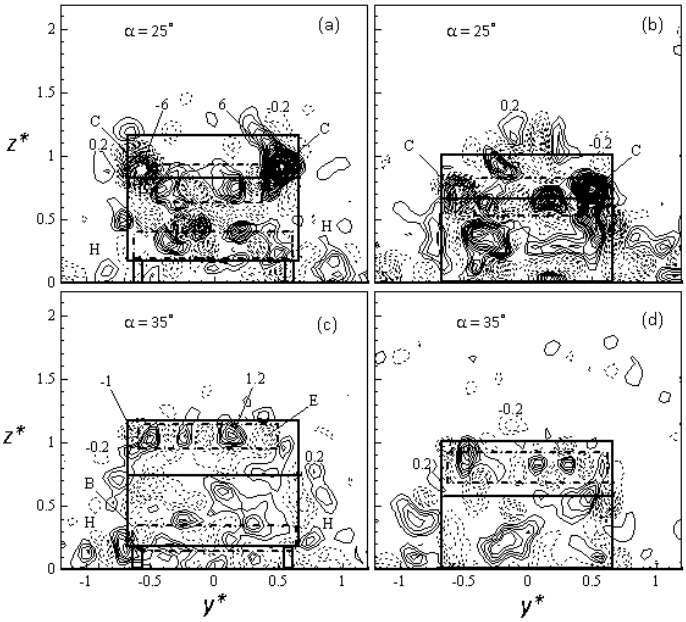

Figure 4 Iso-contours of instantaneous streamwise component, Ω_x^*, of vorticity in the *y*-*z* plane at $x^* = 0.23$ ($Re_H = 5.26\times10^4$): (a, c) $g^* = 0.174$, (b, d) $g^* = 0$. The contour interval is 0.2 and the cutoff level is ± 0.2.

It has been established that the recirculatory bubbles "A" and "B" result from spanwise shedding from the vertical base[5]. Such spanwise structures should be nominally 2-D in the central section, though highly 3-D near their ends. Vino *et al*.[9] measured surface pressure and all three fluctuating components of flow velocity around an Ahmed model at Re_H = 1.2 x 10^5. The spectra of the pressure and velocity signals measured behind the base displayed a pronounced peak at a Strouhal number of about 0.4 based on the square root of model frontal area. This is also confirmed by our hotwire measurements (not shown). The result demonstrates unequivocally the presence of quasi-periodical structures. Furthermore, this peak is by far stronger in the spectra of the streamwise and transverse fluctuating velocities than in the spectrum of the spanwise component, suggesting that the coherent structures were predominantly spanwise oriented. The formation nature of the structures, along with their behaviors, prompts us to connect the structures with the Karman vortex street behind a 2-D bluff body. The latter flow has been extensively studied in the literature, with many aspects of its flow physics unveiled. It is now well known that two major types of vortical structures occur in this flow, i.e., the nominally 2-D spanwise vortices and the predominantly longitudinal rib structures [25, 26]. Evidently, the streamwise vorticity concentrations observed in the base (Figs 3a or 4a) could be a manifestation of the longitudinal rib structures. There is another possibility. Flow visualizations [27, 28] point to a waviness of the spanwise vortices. This has been confirmed by direct numerical simulation (DNS) data [29, 30]. The spanwise vortices can be shed in either parallel or oblique modes[28]. All of these features, *inter alia*, could be associated with the flow structure separated from the upper and lower edges of the base or the upper edge of the slant. A spanwise vortex roll wrapped with rib structures could explain the structures near the lower edge of the base and the upper edge of the slant. On the other hand, in view of the end effects, especially the induction effect of the two C-pillar vortices, the scenario of wavy spanwise rolls is considered to be more likely for the alternately signed structures of relatively larger scale separated from the upper edge of the base, though the possibility that the induction effect of the two C-pillar vortices enhances the rib structures should not be excluded. We will come to this point again when discussing transverse structures in Section 5. On the basis of the present data and previous observations, the schematic representations of the two scenarios are constructed in Fig. 5.

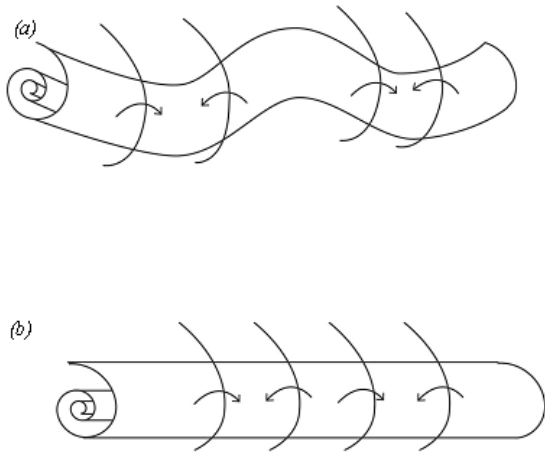

Figure 5 Schematic of the separated spanwise roll wrapped with the rib structures: (a) scenario 1, (b) scenario 2.

4. SPANWISE STRUCTURES

The knowledge of spanwise structures is essential for us to understand thoroughly the highly 3-D flow structure around an Ahmed vehicle model. Figure 6 shows the iso-contours of $\overline{\Omega_y^*}$ in the *x*-*z* plane at $y^* = 0$. At $\alpha = 25°$, the $\overline{\Omega_y^*}$ -contours (Fig 6a and 6b) remain attached to the slant surface, be $g^* = 0$ or not.

Two recirculatory bubbles are evident at $g^* = 0.174$ (Fig 6a), which are separated from the upper and lower edges and are referred to in Section 3 as vortices "A" and "B", respectively, though bubble "B" disappears at $g^* = 0$ (Fig 6b). At $\alpha = 35°$, flow separates from the upper edge of the slant, rather than the lower edge (Fig 6c and 6d). Naturally, the recirculatory bubble "A" is absent. There is a small region of positive $\overline{\Omega_y^*}$ -contours attached to the vertical base at $\alpha = 25°$ or both the slant and vertical base at $\alpha = 35°$, induced by the negative circulation. Recirculatory bubble "B" exhibits a considerably larger strength in terms of the maximum vorticity concentration and size at $\alpha = 35°$ than at $\alpha = 25°$, and the downwash flow is by far stronger at $\alpha = 25°$ than at $\alpha = 35°$, acting to hold bubble "B" down and to restrain its development. It is worth noting that vortex "A" or "B" produces a much higher vorticity concentration in the *x*-*z* plane than in the *y*-*z* plane (Fig 3), suggesting its overwhelmingly spanwise orientation.

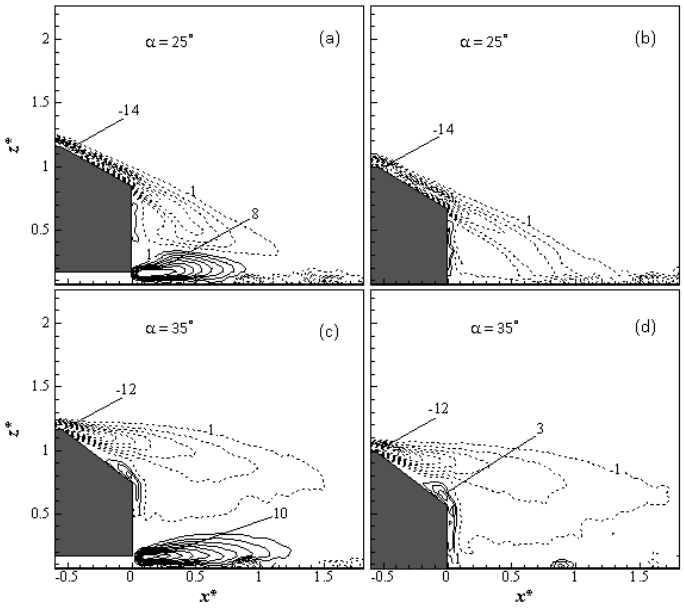

Figure 6 Iso-contours of the averaged spanwise component of vorticity, $\overline{\Omega_y^*}$, in the *x*-*z* plane at $y^* = 0$ ($Re_H = 5.26\times10^4$): (a, c) $g^* = 0.174$, (b, d) $g^* = 0$. The contour interval is 1.0 and the cutoff level is ± 1.

Figure 7 shows iso-contours of averaged streamwise velocity, $\overline{U}^*$ in the *x*-*z* plane at $y^* = 0$. The observation points to that, while part of the shear layer developed over the top of the model remains attached to the slant (Figs 7a), the other part is detached from the body, responsible for the concentrations above the upper edge of the slant, albeit weak, in the $\overline{\Omega_x^*}$-(Figs 3a). At $\alpha = 35°$, the recirculation bubbles over the slant surface "E" and rear of the model "A" are merged into one. Note that in each case there is one blank area near the upper edge of the base, where the u_{rms}^*-contour level is very low. This area corresponds to the stagnant fluid region where $\overline{U}^* \approx 0$ (cf. Fig 7).

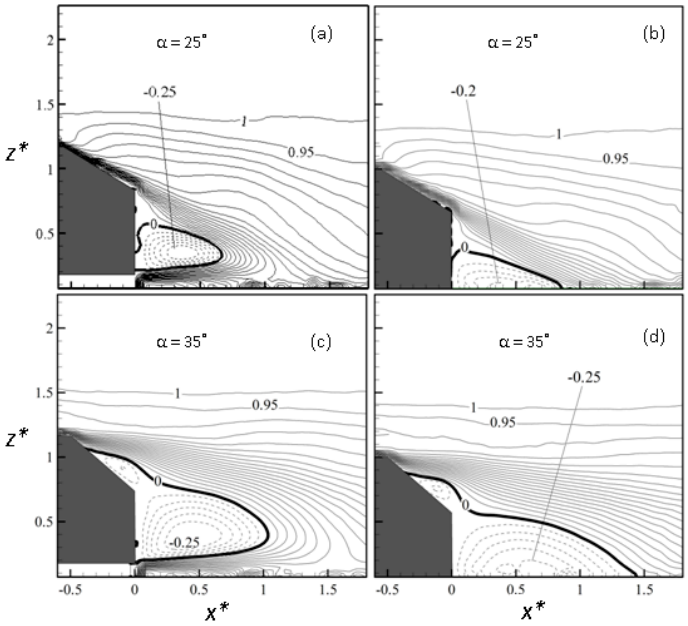

Figure 7 Iso-contours of averaged streamwise velocity, $\overline{U}^*$, in the *x*-*z* plane at $y^* = 0$ ($Re_H = 5.26\times10^4$): (a, c) $g^* = 0.174$, (b, d) $g^* = 0$. The contour interval is 0.05. The cutoff levels are + 1.0 and – 0.05.

5. TRANSCERSE STRUCTURES

The behaviours of the 3-D flow structure in the *x*-*y* plane are investigated by examining the transverse structures of vorticity. The iso-contours of $\overline{\Omega_z^*}$ in the *x*-*y* plane (Fig 8) are approximately symmetrical about $y^* = 0$. At $\alpha = 25°$ and $g^* = 0.174$, three strip structures are seen on each side of $y^* = 0$ in the contours (Fig 8a). The outer strip results largely from vortex "I" and its merging, starting from $x^* \approx 1.0$, with the C-pillar vortex. The middle oppositely signed strip may originate from the interaction between the C-pillar vortex and bubble "A", though the contributions from "I" could not be excluded. The sign of the inner strip is different from that of the middle strip, corroborating our proposition of bubble "A" in Fig 5. There is a blank area between the two inner strips, which meet at about $x^* \approx 0.7$. Spanwise further away from the C-pillar vortex which induces an oppositely signed vorticity concentration (e.g. Fig 4a), those vorticity concentrations in the row of alternately signed structures associated with "A" tend to occur more randomly along the spanwise direction, enhancing the cancelation of each other. At $g^* = 0$ (Fig 8b), a similar flow structure is observed, supporting the assertion that the middle and inner strips are linked with the occurrence of the bubble "A".

At $\alpha = 35°$, the outer strip only is observed in Fig 8c and 8d. This is not unexpected since bubble "A" does not exist;

furthermore, at g* = 0.174, the alternately signed structures associated with "B" are located more randomly along the spanwise direction, promoting the cancelation of each other.

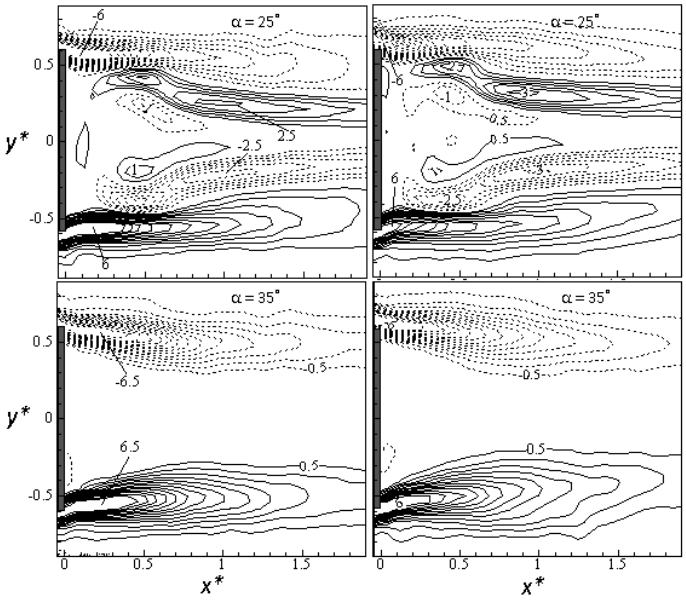

Figure 8 Iso-contours of the averaged vertical component of vorticity, $\overline{\Omega_z}^*$, in the *x*-*y* plane at *z** = 0.59 ($Re_H = 5.26\times10^4$): (a, c) *g** = 0.174, (b, d) *g** = 0. The contour interval is 0.5 and the cutoff level is ± 0.5.

6. SUMMARY AND CONCLUSIONS

The 3-D wake of the Ahmed model, with and without a clearance (g* = 0.174) from wall, has been investigated at $Re_H = 5.26\times10^4$ in detail based on the PIV measurements in three orthogonal planes. Two distinct flow regimes are examined, as represented by the configurations of α = 25° and 35°, respectively. The investigation leads to a number of findings, as summarized and incorporated in the schematic of the flow structure in Figure 9.

In the regime of α < 30°, following modifications are made in Fig 9a:

1 Shear layer developed over the top of the vehicle model flows partially along the slant under the effect of the C-pillar vortex and detaches partially from the body.

2 While part of the shear layer separated from the slant is drawn into recirculation bubble "A", the other part forms a quasi-periodical wavy spanwise roll flowing over "A". The spectra of both fluctuating pressure and velocity signals measured on or behind the upper edge of the vertical base by Vino *et al.*[9] displayed a pronounced peak at a dimensionless frequency of about 0.4 based on the square root of model frontal area. The result was also confirmed by our hotwire measurements, thus providing experimental evidence for quasi-periodical flow separation from the upper edge of the base. This spanwise roll produces alternately signed vorticity concentrations in the *y*-*z* plane (Figs 3a and 4a) and in the *x*-*y* plane (Fig 8a).

3 Separated from the lower edge of the base, the gap flow between the model underside and wall is partially drawn into recirculatory bubble "B" and partially rolls up, forming a spanwise roll that is separated quasi-periodically, again based on Vino *et al.*'s data.[9] This roll is wrapped by longitudinal structures, as is supported by instantaneous longitudinal vorticity contours (Fig 4a).

4 Side vortex "I" is added, which is generated by the shear layer developed over the side surface. This vortex starts breaking down at x* ≈ 1.0 as a result of interaction and merger with the C-pillar vortex.

5 The previously observed lower vortex [10,11] is added, which is generated by the pressure difference between flow inside the gap and that outside, in a manner similar to how the C-pillar vortices are generated.

6 One pair of gap vortices are included, which are generated by struts between the model underside and wall.

In the regime of α > 30°, a flow structure model is presently proposed in Fig 9b, complementing the rather simple model [13], which was constructed based on Lienhardt *et al.*'s data [11], without many details of the flow structure. In the present model, the flow features 3 through 4 at α < 30° apply. Following changes are noted, as per the case of α < 30°:

1 The shear layer developed over the top of the vehicle now separates near the upper edge of the slant (Fig 6c) and is imbedded with alternately signed longitudinal vortices, as evidenced in Figs 3c and 4c.

2 The C-pillar vortex bursts, resulting in a greatly weakened strength, as is discernible in Figs 3c.

3 Recirculation bubbles "E" over the slant and "A" behind the base merge into one (Fig 6c).

A comparison is made between the wakes of the Ahmed model with and without a clearance. The extreme case at g* = 0 eliminates the complication caused by the clearance, serving as an important reference for the understanding of the highly complicated vehicle wake. It is found that this clearance has a pronounced effect on the near wake of the vehicle model. Firstly, both bubbles "A" and "B" are altered in the absence of this clearance (Figs 6b & 6d), including the disappearance of bubble "B". Secondly, the recirculation region that is evident at g* ≠ 0 does not occur at g* = 0, as indicated by the $\overline{U}^*$-contours (Fig 7). Thirdly, the absence of the clearance changes

the strengths of the C-pillar vortex "C" and side vortex "I" (Fig 3).

Finally, the mean velocity and the second moments of fluctuating velocities have been obtained in three orthogonal planes for different configurations, i.e., g* = 0.174 and 0 and α = 25° and 35°, which may be used for the validation of numerical models in the future.

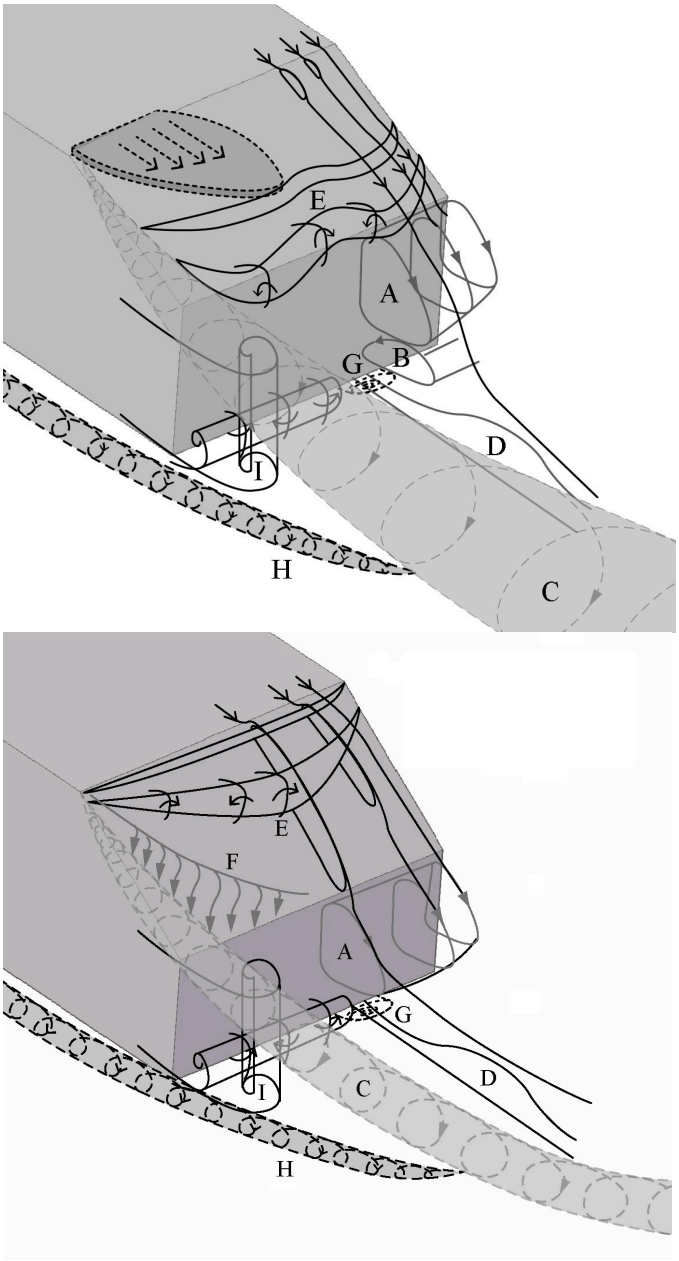

Figure 9 Schematic of flow structure models: (a) α = 25°, (b) 35°.

ACKNOWLEDGEMENTS

YZ wishes to acknowledge support given to him from Research Grants Council of HKSAR through grant PolyU 5329/11E and from The Hong Kong Polytechnic University through grant G-U794.

REFERENCES

[1] Hucho WH & Sovran G, Aerodynamics of Road Vehicles, *Annual Review of Fluid Mechanics,* 1993,Vol. 25, 485-537.

[2] Beaudoin JF, Aider JL, Drag and lift reduction of a 3D bluff body using flaps. *Experiments in Fluids* 44(4) 2008:491-501

[3] Oertel H., Wakes behind blunt bodies. *Annual Review of Fluid Mechanics*, 1990, 22:539-64.

[4] Janssen LJ, Hucho WH, Aerodynamische Formoptimierung der Type VW-Golf und VW-Sirocco. *Kolloquium uber Inderstrie-aerodynamik, Achen,* 1974, Part 3, 46-49.

[5] Ahmed SR, Ramm G, Faltin G., Some salient features of the time averaged ground vehicle wake. *SAE Technical Paper* 1984 No.: 840300, USA.

[6] Brunn A, Wassen E, Sperber D, Nitsche W, Thiele F,. Active drag control for a generic car. *In Active Flow Control (ed. King R),* 2007 NNFM95, 247-259, Springer-Verlag Berlin Heidelberg.

[7] Sims-Williams DB, Dominy RG, Howell JP, An investigation into large scale unsteady structures in the wake of real and idealized hatchback car models. *SAE Technical Paper* 2001 No.: 2001-01-1041.

[8] Sims-Williams, DB, Self-Excited Aerodynamic Unsteadiness Associated with Passenger Cars, PhD Thesis, University of Durham. 2001

[9] Vino, G., Watkins, S., Mousley, P., Watmuff, J., Prasad, S. Flow structures in the near-wake of the Ahmed model. *Journal of Fluids and Structure* 2005 20:673-695.

[10]. Krajnovic S, Davidson L, Flow around a simplified car, Part 1: large eddy simulation. *ASME Journal of Fluids Engineering* 2005a 127:907-918.

[11] Strachan RK, Knowles K., Lawson NJ, The vortex structure behind an Ahmed reference model in the presence of a moving ground plane. *Experiments in Fluids*, 2007, 42: 659-669.

[12] Sims-Williams DB, Duncan BD, The Ahmed model unsteady wake: Experimental and computational analyses. *SAE Technical Paper* 2003, No.: 2003-01-1315.

[13] Lienhart H, Becker S, Flow and turbulence structures in the wake of a simplified car model. *SAE Technical Paper* 2003No.: 2003-01-0656.

[14]. Krajnovic S, Davidson L Flow around a simplified car, Part 2: understanding the flow. *ASME Journal of Fluids Engineering* 2005b 127:919-928.

[15] Krajnovic S, Davidson L, Exploring the flow around a simplified bus with large eddy simulation and topological tools, in *The Serodynamics of Heavy Vehicles: Trucks, Buses and Trains* 2002 (Springer, Monterey, CA).

[16] Krajnovic S, Davidson L, Numerical study of the flow around the bus-shaped body, *ASME Journal of Fluids Engineering,* 2003 125, 500-509.

[17] Huang J F, Zhou Y & Zhou T M, Three-dimensional wake structure measurement using a modified PIV technique, *Experiments in Fluids* 2006 40, 884-896.

[18] Farell C, Carrasquel S, Guben O, Patel VC, Effect of wind tunnel walls on the flow past circular cylinders and cooling tower models. *Journal Fluids Engineering* 1977 99:470-479.

[19] Narasimha R, Prasad SN, Leading edge shape for flat plate boundary layer studies. *Experiments in Fluids*, 1994 17:358-360.
[20] Thacker A, Aubrun S, Leroy A, Devinant P, Unsteady analyses of the flow separation on the rear window of a simplified ground vehicle model, *AIAA paper* 2010-4569.
[21] Joseph P, Amandolese X, Aider JL Drag reduction on the 25^{o} slant angle Ahmed reference body using pulsed jets. *Experiments in Fluids*: 2011.
[22] Wang HF, Zhou Y, Chan CK and Lam KS, Effect of initial conditions on interaction between a boundary layer and a wall-mounted finite-length-cylinder wake. *Physics of Fluids* 18: 2006 Art. No. 065106.
[23]. Zhang H.J., Zhou Y., Whitelaw J.H., Near-field wing-tip vortices and exponential vortex solution. *Journal. of Aircraft* 2006 43:446-449.
[24] Minguez M, Pasquetti R, Serre E, Spectral vanishing viscosity stabilized LES of the Ahmed body turbulent wake. *Communication in Computational Physics*, 2009 5(2-4): 635-648
[25]. Zhou Y, Antonia RA, Critical points in a turbulent near wake. *Journal of Fluid Mechanics* 1994 275, 59-81.
[26] Zhang H.J., Zhou, Y. & Antonia, R.A., Longitudinal and spanwise structures in a turbulent wake, *Physics of Fluids*, 2000 12, 2954-2964.
[27] Wu J, Sheridan J, Welsh MC and Hourigan K, Three-dimensional vortex structures in a cylinder wake, *The Journal of Fluid Mechanics.* 1996 312, 201.
[28] Williamson CHK, Vortex dynamics in the cylinder wake, *Annual Review of Fluid Mechanics.* 1996 28, 477.
[29] Thompson M, Hourigan K, Sheridan J, Three-dimensional instabilities in the cylinder wake, *Proceedings International Colloquium on Jets, Wakes and Shear Layers, Melbourne, Australia*, 18-20 April 1994.
[30] Zhang H-Q, Fey U, Noack BR, König M & Eckelmann H, On the transition of the cylinder wake, *Physics of Fluids* 1995 7, 779.